2026 IEEE International Conference on Robotics and Automation (ICRA 2026)
June 1-5, 2026. Vienna, Austria

The Actuator Pre-Filtering Approach to Control-Coherent Koopman LQR for Robot Systems Interacting with Compliant Environment

Jasmine Terrones and H. Harry Asada, *Life Fellow*

***Abstract*— As a robot makes and breaks contact with environment surfaces, the equations of motion are switched. Task planning and real-time control become challenging as the system traverses multiple regions and switches the governing dynamics. This paper presents a modeling and real-time control methodology for such switched dynamical systems based on Koopman operator theory. Potentially, Koopman operators allow us to subsume segmented dynamics within a unified, globally linear model amenable for control analysis and synthesis. However, the original Koopman operators are not appliable to non-autonomous systems with exogenous input. A new method for converting robot dynamics to a Koopman-compatible model using actuator pre-filtering is presented and applied to the modeling and control of robots interacting with the environment. Specifically, an underactuated cart-pole robot bouncing against multiple walls is modeled as a Control-Coherent Koopman model and a Koopman LQR controller is designed for the wall-bouncing robot. Simulation experiments demonstrate the effectiveness of the method and investigates the effect of the actuator pre-filter parameter on control performance.**

***Index Terms*— Koopman lifting linearization, Koopman operator for control systems, Actuator prefilter, Koopman LQR**

I. Introduction

Contact with the environment is essential in all kinds of robotic tasks, including leg locomotion [1,2] and contact-rich manipulation [3,4]. As a robot dynamically engages with the environment, it makes and breaks contact with constraining surfaces, and its governing equations are switched. Unfortunately, task planning and real-time control become challenging, as the dynamics switch at the contact boundaries. The objective of the current work is to explore a new modeling and representation methodology for dealing with switched dynamical processes so that planning and control can be performed effectively. Specifically, we aim to unify segmented dynamics and subsume them within a global model amenable for real-time planning and control [5].

Koopman operators can represent nonlinear dynamical processes as a globally linear dynamic equation in a high-dimensional state space [6,7,8,9]. Here, we use the Koopman operator theory as a means for aggregating segmented dynamics and subsuming them within a unified, globally linear model. The benefit of converting otherwise complex segmented dynamics to a unified, globally linear model is significant. Complex nonlinear optimization and mixed-integer optimization can be reduced to straightforward, convex optimization. This can significantly reduce computation time, eliminate local minima, and resources required.

Despite the salient features of Koopman modeling and control, fundamental drawbacks and limitations of the application of Koopman operators remain. The original Koopman operator theory is applicable only to autonomous systems with no exogenous input [1]. Almost all control systems are non-autonomous with control, to which the Koopman theory does not apply in the strict sense. This fundamental gap causes erroneous control synthesis, limited prediction accuracy, and limits the applicability of Koopman-based modeling.

In robotics and control literature, a few methods have been developed to alleviate the limitation. These include a) Dynamic Mode Decomposition with control (DMDc), which approximates a state-dependent control gain matrix to a constant matrix [10], b) a method for treating input variables as state variables [11], c) a method for constructing the multitude of Koopman operators and control gain matrices for different values of control inputs, and d) the bilinear approximation of the state-dependent control gain matrix [12,13]. DMDc is applicable only to cases where the state-dependent control gain matrix does not vary significantly. Methods b) and c) are useful for processes with known feedback control or the cases where control input can take a limited set of specific values. In control synthesis, however, it is required to take an arbitrary control action. Therefore, these methods do not fit the requirements for real-time control. The bilinear approximation provides a better prediction accuracy, but the model is no longer globally linear.

An emerging method, termed Control-Coherent Koopman (CCK) modeling, allows us to construct a Koopman model with a constant control matrix that is valid globally [14]. The method incorporates dynamics of actuators into the plant dynamics to construct a model that is coherent with the original Koopman operator theory. Dynamics of an actuator powertrain, for example, exhibits some mechanical compliance. As a result, the actuator and its load possess independent states. It has been shown that, if control terms appear linearly in the actuator dynamics equations, a Control-Coherent Koopman model can be constructed [14]. No approximation is required for obtaining the globally linear control matrix. Integrity and coherency of the input matrix are crucial for proper control design. The new method guarantees the coherent, correct structure of the control matrix.

[1]This manuscript was submitted on September 16, 2025, for review. This material is based upon work supported by the National Science Foundation under Grant No. NSF-CMMI 2021625.

Jasmine Terrones and Harry H. Asada are with Department of Mechanical Engineering, Massachusetts Institute of Technology, Cambridge, MA 02139 USA. * is the corresponding author (e-mail: jterrone@mit.edu*, asada@mit.edu).

Augmenting state equations by modeling the compliance between actuators and their load provides us with a model that is coherent with the Koopman operator theory. Nonetheless, the method is applicable only to a class of systems having specific physical properties. Recently, the principle of CCK modeling has been extended to those systems where actuator dynamics do not possess independent state variables, violating a key requirement for the CCK formulation. In the new formulation, physical actuator dynamics are replaced by virtual dynamics, possessing independent state variables and new input terms that appear linearly in the virtual dynamics [15]. This is equivalent to an actuator pre-filter through which actuator commands are conditioned and transmitted to the physical actuator. Although the original CCK physical modeling approach suffers a stiff equation problem, the actuator pre-filtering approach does not. It is applicable to broader control systems and provides greater flexibility in the use of Koopman operators.

In this paper, the actuator pre-filtering approach to constructing CCK models is applied to switched dynamical systems. Segmented dynamics due to making and breaking contact with environment surfaces will be reduced to a unified, globally linear model. Optimal control is designed for the unified, globally linear system, and the parameters of the actuator pre-filters are studied. Code, videos, and details at github.com/jterrone1/ICRA2026_actuator_prefilter_cartpole

II. Preliminary Work

This section summarizes Koopman operator theory and Control-Coherent Koopman modeling as background information for readability of the paper. For more details, the reader is directed to references [5, 6, 7, 14].

A. Koopman Operators

Consider a discrete-time, autonomous nonlinear system with no exogenous input:

$$\boldsymbol{x}_{t+1} = F(\boldsymbol{x}_t) \tag{1}$$

where $\boldsymbol{x}_t \in X \subset \mathbb{R}^n$, and function F is a self-map, $F: X \mapsto X$, which is continuous.

Let $\{\varphi_i(\boldsymbol{x}_t)\}_{i=1}^{\infty}$ be orthonormal basis functions that span a Hilbert space $\mathcal{H}$. Assume that the basis functions compositional with the self-map F are involved in the Hilbert space.

$$\varphi_i \circ F \in \mathcal{H}, \quad i = 1,2,\cdots \tag{2}$$

Then, the function $\phi_i \circ F$ can be expanded to a series of the orthonormal basis functions.

$$\varphi_i \circ F = \sum_{j=1}^{\infty} \langle \varphi_i \circ F, \varphi_j \rangle \varphi_j \tag{3}$$

where $\langle -, - \rangle$ represents the inner product of two functions. Note that, from (1), we find that

$$(\varphi_i \circ F)(\boldsymbol{x}_t) = \varphi_i(F(\boldsymbol{x}_t)) = \varphi_i(\boldsymbol{x}_{t+1}) \tag{4}$$

Namely, the function $\varphi_i \circ F$ evaluated at state $\boldsymbol{x}_t$ represents the observables at the next state $\boldsymbol{x}_{t+1}$. Now consider the state $\boldsymbol{x}_t$ viewed from the infinite number of basis functions, called observables, $\bar{\boldsymbol{z}}_t = (\varphi_1(\boldsymbol{x}_t), \varphi_2(\boldsymbol{x}_t), \cdots)^T$. From (3) and (4), we can find that

$$\bar{\boldsymbol{z}}_{t+1} = \bar{\mathrm{A}}\bar{\boldsymbol{z}}_t \tag{5}$$

where

$$\bar{\mathrm{A}} = \begin{bmatrix} \langle \varphi_1 \circ F, \varphi_1 \rangle & \langle \varphi_1 \circ F, \varphi_2 \rangle & \cdots \\ \langle \varphi_2 \circ F, \varphi_1 \rangle & \langle \varphi_2 \circ F, \varphi_2 \rangle & \cdots \\ \vdots & \vdots & \ddots \end{bmatrix}. \tag{6}$$

Representing the state with the infinite number of observables, $\bar{\boldsymbol{z}}_t$, we can interpret (5) as a state transition equation in the infinite dimensional space. Note that this state transition is "globally" linear, strikingly different from the standard pointwise linearization, which is valid only in the vicinity of the point.

While the orthonormal basis functions were used for representing the state, more general basis functions can be used for the state transition, if the basis functions span the Hilbert space.

$$\boldsymbol{z}_{t+1} = \mathrm{A}\boldsymbol{z}_t \tag{7}$$

where $\boldsymbol{z}_t = (g_1(\boldsymbol{x}_t), g_2(\boldsymbol{x}_t), \cdots)^T$ is the infinite-dimensional state lifted with observables $\{g_i\}_{i=1}^{\infty}$, which are not necessarily orthonormal but are independent [5].

Post-multiply $\boldsymbol{z}_t{}^T$ to both sides of (7) and integrate them over the dynamic range of the independent state yields

$$\mathrm{Q} = \mathrm{AR} \tag{8}$$

where

$$\mathrm{Q} = \langle \boldsymbol{z}_{t+1}, \boldsymbol{z}_t^T \rangle = \left\{ \int_X g_i[F(\boldsymbol{x})] \cdot g_j(\boldsymbol{x}) d\boldsymbol{x} \right\} \tag{9}$$

$$\mathrm{R} = \langle \boldsymbol{z}_t, \boldsymbol{z}_t^T \rangle = \left\{ \int_X g_i(\boldsymbol{x}) \cdot g_j(\boldsymbol{x}) d\boldsymbol{x} \right\} \tag{10}$$

The Koopman operator is the solution to the linear equation (7). This method for obtaining the Koopman operator is called Koopman Direct Encoding [5]. Finding an effective set of observables is a challenge, but deep learning has been used for constructing them from data [16].

B. Control-Coherent Koopman Modeling

The above Koopman operators are for autonomous systems with no control input. Now consider a non-autonomous system with exogenous input.

$$\boldsymbol{x}_{t+1} = f(\boldsymbol{x}_t, \boldsymbol{u}_t) \tag{11}$$

where $\boldsymbol{u}_t \in U \subset \mathbb{R}^r$ is the input, and f is a continuously differentiable function, $f: X \times U \to X$ defined in compact subsets X and U. Our goal is to obtain a Koopman lifted linearization method for the non-autonomous system (11) in the following form:

$$\boldsymbol{z}_{t+1} = \mathrm{A}\boldsymbol{z}_t + \mathrm{B}\boldsymbol{u}_t \tag{12}$$

which is linear in control $\boldsymbol{u}_t$ with a constant input matrix B.

In general, it is impossible to obtain the globally linear, time-invariant model (12). However, the linear non-autonomous system model exists for a class of nonlinear systems that can be reduced to a Koopman-compatible expression. This section briefly describes such a method,

called Control-Coherent Koopman modeling, based on [14].

The key concept of Control-Coherent Koopman modeling is to divide the state space into one associated to a set of state variables $\boldsymbol{p}_t \in P \subset \mathbb{R}^m$ that is driven directly with input u_t and the rest of the state variables $\boldsymbol{q}_t \in X_q \subset \mathbb{R}^{n-m}$ that are not directly driven by $\boldsymbol{u}_t$ but indirectly through $\boldsymbol{p}_t$.

$$\boldsymbol{x}_t = \begin{bmatrix} \boldsymbol{p}_t \\ \boldsymbol{q}_t \end{bmatrix}, \quad \boldsymbol{p}_t \in P \subset \mathbb{R}^m, \boldsymbol{q}_t \in X_q \subset \mathbb{R}^{n-m} \tag{13}$$

State $\boldsymbol{p}_t$ is called actuator state, while state $\boldsymbol{q}_t$ is called plant state. Each has a nonlinear state transition equation. The CCK modeling is possible for a particular class of nonlinear dynamical systems where all the control input terms appear linearly in the state transition equation of the actuator dynamics, and the plant state is not directly driven by the input:

$$\boldsymbol{p}_{t+1} = f_p(\boldsymbol{p}_t, \boldsymbol{q}_t, \boldsymbol{u}_t) = \bar{f}_p(\boldsymbol{p}_t, \boldsymbol{q}_t) + \mathrm{B}_p \boldsymbol{u}_t \tag{14}$$

$$\boldsymbol{q}_{t+1} = f_q(\boldsymbol{p}_t, \boldsymbol{q}_t) \tag{15}$$

where $f_q : P \times X_q \mapsto X_q \subset \mathbb{R}^{n-m}$ and $f_p : P \times X_q \times U \mapsto P$ are continuously differentiable, and $\mathrm{B}_p \in \mathbb{R}^{n \times r}$ is a constant matrix.

For this class of systems, a globally linear state transition equation (12) can be obtained by first generating the Koopman operator for the associated autonomous system. Setting $\boldsymbol{u}_t \equiv 0$ in (14),

$$\boldsymbol{p}_{t+1} = \bar{f}_p(\boldsymbol{p}_t, \boldsymbol{q}_t) \tag{16}$$

$$\boldsymbol{q}_{t+1} = f_q(\boldsymbol{p}_t, \boldsymbol{q}_t)$$

If a Koopman operator exists for compact subsets $\boldsymbol{q}_t \in X_q$ and $\boldsymbol{p}_t \in P$, where all the actuator states $\boldsymbol{p}_t$ driven by the input $\boldsymbol{u}_t \in U$ according to (11) are contained,

$$f_p(\boldsymbol{p}, \boldsymbol{q}, \boldsymbol{u}) \in P, \ \forall \boldsymbol{q} \in X_q, \forall \boldsymbol{u} \in U, \forall \boldsymbol{p} \in P \tag{17}$$

the operator is called the Extended Autonomous Koopman Operator of the control system (14) and (15). The CCK mode of this system can be constructed as stated in the following Proposition.

Proposition [Control-Coherent Koopman Model]

If a discrete-time dynamical system possessing an actuator subsystem has an Extended Autonomous Koopman operator with observables $\{g_i\}_{i=1}^{\infty}$ that contain the state variables of the actuation subsystem, $\boldsymbol{p}$, in the observables, and the actuation subsystem is linear in actuation in the form of (14), then a Control-Coherent Koopman Model exists and is given by

$$\boldsymbol{z}_{t+1} = \mathrm{A}\boldsymbol{z}_t + \mathrm{B}\boldsymbol{u}_t.$$

where $\boldsymbol{z}_t$ is lifted state with $\boldsymbol{p}$ in the first m observables:

$$\boldsymbol{z}_t = \begin{bmatrix} \boldsymbol{p}_t \\ \boldsymbol{y}_t \end{bmatrix} \text{ with } \boldsymbol{y}_t = (g_{m+1}, g_{m+2}, \cdots)^T. \tag{18}$$

A is the Extended Autonomous Koopman operator, and B is a constant control matrix, given by:

$$\mathrm{A} = \begin{bmatrix} \mathrm{A}_{pp} & \mathrm{A}_{py} \\ \mathrm{A}_{yp} & \mathrm{A}_{yy} \end{bmatrix} \text{ and } \mathrm{B} = \begin{bmatrix} \mathrm{B}_p \\ 0 \end{bmatrix} \tag{19}$$

The actuation subsystem and the plant subsystem must have algebraically independent state variables $\boldsymbol{p}$ and $\boldsymbol{q}$, although these subsystems are dynamically coupled. The actuator dynamics must have control input terms that appear linearly. These requirements can be met as addressed next.

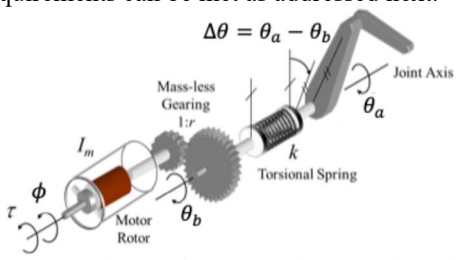

Fig.1 Powertrain model of a robot. Due to the torsional compliance at the transmission, the actuator displacement ϕ and the joint displacement θ_a are independent generalized coordinates, i.e. independent states.

III. Control-Coherent Koopman Modeling of Robot Systems Interacting with Environment Surfaces

This section presents a Control-Coherent Koopman formulation of a general n_r Degrees of Freedom (DoF) robot based on the actuator pre-filtering approach. First, we deal with a robot having no physical interaction with the environment, followed by the one with contacts with external walls.

A. Control-Coherent Koopman Modeling Using Actuator Pre-Filtering

Fig. 1 shows an n_r degree-of-freedom (DoF) serial link robot arm with the equations of motion (EoM) in joint coordinates $\boldsymbol{\theta} \in \mathbb{R}^{n_r}$ given by

$$\mathrm{H}(\boldsymbol{\theta})\ddot{\boldsymbol{\theta}} + \mathrm{C}(\boldsymbol{\theta}, \dot{\boldsymbol{\theta}})\dot{\boldsymbol{\theta}} + \mathrm{G}(\boldsymbol{\theta}) = \boldsymbol{\tau}_J \tag{20}$$

where $\mathrm{H}(\boldsymbol{\theta})$ is an $n_r \times n_r$ inertia matrix, $\mathrm{C}(\boldsymbol{\theta}, \dot{\boldsymbol{\theta}})$ is the Coriolis and centrifugal matrix, $\mathrm{G}(\boldsymbol{\theta})$ is the gravity vector, and $\boldsymbol{\tau}_J \in \mathbb{R}^{r_r}$ is the joint torque vector [17]. If we define $\boldsymbol{\theta}$ and $\dot{\boldsymbol{\theta}}$ to be independent state variables, the state equation can be given by

$$\frac{d}{dt}\begin{pmatrix} \boldsymbol{\theta} \\ \dot{\boldsymbol{\theta}} \end{pmatrix} = \begin{bmatrix} \dot{\boldsymbol{\theta}} \\ \mathrm{H}(\boldsymbol{\theta})^{-1}\boldsymbol{\tau}_J - \mathrm{H}(\boldsymbol{\theta})^{-1}\left(\mathrm{C}\dot{\boldsymbol{\theta}} + \mathrm{G}(\boldsymbol{\theta})\right) \end{bmatrix} \tag{21}$$

In most robotics literature, joint torques $\boldsymbol{\tau}_J(t)$ are treated as control input. In consequence, the state equation is not linear in control; the joint torques are multiplied by the inverse of the state-dependent inertia matrix, $\mathrm{H}(\boldsymbol{\theta})^{-1}$. The Koopman operator theory cannot be applied to this form of dynamical system.

This governing equation can be reframed to fit the Control-Coherent Koopman framework by considering its actuator dynamics. As described in the previous section, Control-Coherent Koopman model can be obtained if two physical properties are met. One is that actuator subsystem dynamics possess independent state variables, and the other is

that a control term appears linearly in each actuator subsystem. As shown in Fig. 1, these conditions can be met if the powertrain of each joint actuator, comprising a gearing and transmission mechanism, possesses significant compliance. Serial elastic actuators and powertrains with flexible transmissions, such as Harmonic Drives, yield torsional displacements between the actuator-side axis and the load-side axis, each possessing independent state variables. However, no significant torsional displacement exists as the powertrain rigidity increases. Direct-Drive and semi-direct drive as well as planetary gears and other high rigidity transmissions do not produce significant torsional displacement. Therefore, the CCK modeling based on the physical compliance of powertrains is not applicable to these robot systems.

Here, we consider an alternative approach to CCK formulation. The two CCK conditions can be satisfied by considering dynamic filters through which control signals are transmitted to physical actuators. As shown in Fig.2, we consider a linear filter in discrete-time,

$$\boldsymbol{w}_{t+1} = \mathrm{A}_w \boldsymbol{w}_t + \mathrm{B}_w \boldsymbol{u}_t \tag{22}$$

$$\boldsymbol{\tau}_{Jt} = \mathrm{C}_w \boldsymbol{w}_t \tag{23}$$

where $\boldsymbol{w}_t \in \mathbb{R}^m$ is the state of the linear filter, $\boldsymbol{u}_t$ is a new input, which appears linearly in the filter dynamics, and $\mathrm{C}_w \in \mathbb{R}^{r\times m}$ is a constant matrix. Replacing the independent actuator state $\boldsymbol{p}_t$ by the filter state $\boldsymbol{w}_t$, we can form a Control-Coherent Koopman model, which is given by

$$\begin{bmatrix}\boldsymbol{w}_{t+1}\\ \boldsymbol{y}_{t+1}\end{bmatrix} = \begin{bmatrix}\mathrm{A}_w & 0\\ \mathrm{A}_{yp} & \mathrm{A}_{yy}\end{bmatrix}\begin{bmatrix}\boldsymbol{w}_t\\ \boldsymbol{y}_t\end{bmatrix} + \begin{bmatrix}\mathrm{B}_w\\ 0\end{bmatrix}\boldsymbol{u}_t, \tag{24}$$

where $\mathrm{A}_w \in \mathbb{R}^{m\times m}$ and $\mathrm{B}_w \in \mathbb{R}^{m\times r}$ are constant system and control matrices, respectively. The observables in (24) are $[g_1, \cdots, g_m] = \boldsymbol{w}^T$, $\boldsymbol{y}_t^T = [g_{m+1}(\boldsymbol{w}_t, \boldsymbol{q}_t), g_{m+2}(\boldsymbol{w}_t, \boldsymbol{q}_t), \cdots]$.

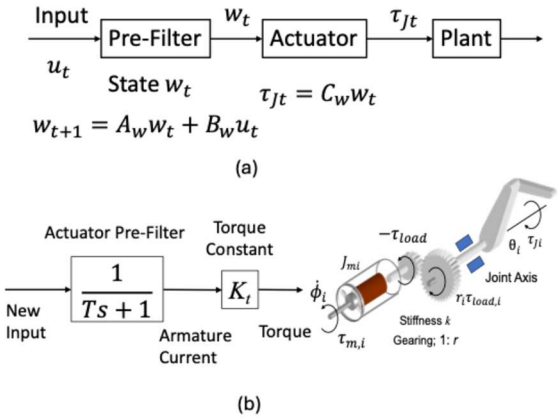

Fig.2 Actuator pre-filter. (a) Block diagram with new input u_t, filter state w_t (b) a first-order pre-filter for electromagnetic actuator with torque constant K_t.

The actuator pre-filtering approach is a direct extension of the physical model-based approach, where the actuator dynamics are replaced by the filter dynamics, which are linear in both state and control terms. This makes the upper right block of the A matrix zero as the filter is linear.

The above state equation (24) manifests that the actuator pre-filter input u_t drives the pre-filter state to $\boldsymbol{w}_{t+1}$ and that all others in y are affected only through $\boldsymbol{w}_{t+1}$ at the *next cycle*, $t+2$. The effect of the input $\boldsymbol{u}_t$ is captured and confined within the pre-filter dynamics in the first cycle, $t \to t+1$, before being transmitted to the dynamics of $\boldsymbol{y}_t$ in the second cycle, $t+1 \to t+2$. If the actuator pre-filter state $\boldsymbol{w}_t$ is eliminated, it implies that this transmission delay is eliminated. As a result, (22) becomes algebraic and the input is directly involved in the plant dynamics (15), which prevents the application of Koopman Operator. The pre-filter must possess independent state variables.

Example [A Pre-Filter for Electromagnetic Actuators]

Consider an electromagnetic actuator that can be treated as a torque Source, where the output torque is proportional to a current to windings, $\tau = K_T i$, and the actuator is driven by an amplifier that can drive sufficient current to the actuator regardless of the state of the load. The current command *i* can be generated with a linear filter, such as

$$i_{t+1} = -a i_t + b u_t \tag{25}$$

The current i_t is treated as an actuator state, $w_t = i_t$, that is driven by input u_t. The actuator output is the torque, τ_{Jt}, and $C_w = K_T$. This actuator pre-filter has its own state that is independent, and the input to the filter u_t appears linearly in the filter dynamics. Therefore, this satisfies the requirements for the Control-Coherent Koopman modeling.

B. CCK Modeling of Robots Interacting with Friction-less Walls

Consider a robot system interacting with friction-less, compliant walls of the environment. The governing equation of motion of a robot contacting with n_w walls is given by

$$\mathrm{H}(\boldsymbol{\theta})\ddot{\boldsymbol{\theta}} + \mathrm{C}\big(\boldsymbol{\theta}, \dot{\boldsymbol{\theta}}\big)\dot{\boldsymbol{\theta}} + \mathrm{G}(\boldsymbol{\theta}) = \boldsymbol{\tau}_J - \mathrm{J}_C \boldsymbol{F}_C \tag{26}$$

where $\boldsymbol{F}_C$ is normal contact forces, $\boldsymbol{F}_C = \big(\boldsymbol{F}_{C1}, \cdots, \boldsymbol{F}_{Cn_w}\big)^T$, and J_C is an $n_r \times n_w$ Jacobian matrix relating the joint coordinates to the contacting points. Each wall is compliant with a stiffness k_{wi} relating the contact force $\boldsymbol{F}_{Ci}$ to penetration s_{wi}.

$$F_{Ci} = \max[k_{wi} s_{wi}, 0] \tag{27}$$

Note that $F_{Ci} \geq 0$. The robot makes and breaks contact with each wall. Depending on its configuration relative to the walls, the governing equations of motion are segmented.

These segmented dynamics can be subsumed within a single, unified, and globally linear system with the use of a Koopman operator. Such a globally linear representation of the switched dynamics facilitates control design. Note that the walls are assumed compliant. Therefore, there is no discontinuity in this system as the robot makes and breaks contact with the walls. Although the system is highly

nonlinear and complex, it can be converted to a globally linear model in a lifted space.

A CCK model is constructed with the following procedure:

1) Convert the above equations of motion to discrete-time state equations.

$$\boldsymbol{q}_{t+1} = f_q(\boldsymbol{\tau}_{Jt}, \boldsymbol{q}_t) \tag{28}$$

2) Determine the actuator pre-filter with filter state $\boldsymbol{w}_t$ and parameter matrices, A_w, B_w, and C_w, and replace $\boldsymbol{\tau}_{Jt}$ by $\mathrm{C}_w\boldsymbol{w}_t$. Also, determine the dynamic range of $\boldsymbol{w}_t$ based on (22), where $\boldsymbol{u}_t \in U$.

3) Setting $\boldsymbol{u}_t = \boldsymbol{0}$, generate a data set for obtaining the Koopman operator of the associated autonomous system:

$$D = \{(\boldsymbol{q}_t, \boldsymbol{w}_t)|t = 0, \cdots, N\} \tag{29}$$

4) Determine M observable functions and compute

$$\boldsymbol{y}_t^T = [g_{m+1}(\boldsymbol{w}_t, \boldsymbol{q}_t), \cdots, g_M(\boldsymbol{w}_t, \boldsymbol{q}_t)] \tag{30}$$

5) Obtain the two block matrices of the A matrix of the associated Extended Autonomous Koopman operator.

$$(\mathrm{A}_{yw}, \mathrm{A}_{yy}) = \underset{\mathrm{A}_{yw},\mathrm{A}_{yy}}{\operatorname{argmin}} \sum \left|\boldsymbol{y}_{t+1} - \left(\mathrm{A}_{yw}\boldsymbol{w}_t + \mathrm{A}_{yy}\boldsymbol{y}_t\right)\right|^2 \tag{31}$$

where $\boldsymbol{y}_{t+1}^T = [g_{m+1}(\bar{\boldsymbol{w}}_{t+1}, \boldsymbol{q}_{t+1}), \cdots, g_M(\bar{\boldsymbol{w}}_{t+1}, \boldsymbol{q}_{t+1})]$ with $\bar{\boldsymbol{w}}_{t+1} = \mathrm{A}_w\boldsymbol{w}_t$, which excludes $\boldsymbol{u}_t$.

6) Construct the system matrix A and the control matrix B as in (24).

IV. Control-Coherent Koopman LQR of a Wall-Bouncing Cart-Pole

The actuator pre-filtering approach to Control-Coherent Koopman modeling is now applied to the cart-pole system bouncing between walls of the environment. Previous studies have analyzed the ability of Koopman models to capture dynamic viscoelastic contact by using radial basis functions to represent localized contact surfaces [18]. We build off this work by using the same observable functions and utilizing actuator prefilter states to generate Koopman LQR controllers.

Fig. 3 shows the schematic of a cart-pole system interacting with a pair of walls. The system consists of a cart with traction force F, a pole attached to the cart with a torsional spring (k) and damper (b). Let m_c be the mass of the cart and m_p be the point mass at the end of the pole. The length of the pole is ℓ, and the moment of inertia of the pole is negligible. The two vertical walls are symmetrically spaced about the coordinate origin O. The wall is compliant, with a spring constant k_w and no damping. The friction on the wall surfaces is negligibly small. All parameter values can be found on GitHub.

The x coordinate of the cart x_C and the pole angle θ_P are used as generalized coordinates $\boldsymbol{\theta} = [x_c, \theta_p]^T$. The plant state variables are $\boldsymbol{q} = [x_c, \theta_p, \dot{x_c}, \dot{\theta_p}]^T$ and the actuator pre-filter state is scalar $w = [F]$.

We consider a first-order pre-filter with time constant T, which is the simplest filter that meets the requirements for actuator prefiltering.

$$\dot{w} = \dot{F} = \frac{1}{T}u - \frac{1}{T}F \tag{32}$$

The equation of motion of the plant is given by

$$\mathrm{H}(\boldsymbol{\theta})\ddot{\boldsymbol{\theta}} + \mathrm{C}(\boldsymbol{\theta}, \dot{\boldsymbol{\theta}}) + \mathrm{G}(\boldsymbol{\theta}) = \mathrm{J}_c(\boldsymbol{\theta})\boldsymbol{F}_C(\boldsymbol{\theta}) + \boldsymbol{b}_\theta(\dot{\boldsymbol{\theta}}) + \mathrm{J}_F F \tag{33}$$

The effects of the control input u are linear and affine with constant coefficients in the pre-filter dynamics. However, the effects of traction F applied to the plant dynamics is not linear due to the *state dependent inertia matrix*. For this reason, a least squares approximation to obtain the control input B matrix would be insufficient in generating a globally accurate Koopman model. This key problem is eliminated with the inclusion of the actuator prefilter dynamics.

$$\mathrm{H}(\boldsymbol{\theta}) = \begin{bmatrix} m_c + m_p & -l\, m_p \cos(\theta_p) \\ -l m_p \cos(\theta_p) & l^2 m_p \end{bmatrix} \tag{34}$$

$$\mathrm{C}(\boldsymbol{\theta}, \dot{\boldsymbol{\theta}}) = \begin{bmatrix} \dot{\theta}_p^2\, l m_p \sin(\theta_p) \\ 0 \end{bmatrix} \tag{35}$$

$$\mathrm{G}(\boldsymbol{\theta}) = \begin{bmatrix} 0 \\ -g\, l m_p \sin(\theta_p) \end{bmatrix} \tag{36}$$

The wall reaction force $\boldsymbol{F_C}$ and the traction force F are transmitted through the following Jacobians,

$$\mathrm{J}_C(\boldsymbol{\theta}) = \begin{bmatrix} 1 & -l\cos(\theta_p) \\ 0 & -l\sin(\theta_p) \end{bmatrix} \tag{37}$$

$$\mathrm{J}_F = \begin{bmatrix} 1 \\ 0 \end{bmatrix} \tag{38}$$

The damping term is given as follows,

$$\boldsymbol{b}_\theta(\dot{\boldsymbol{\theta}}) = \begin{bmatrix} 0 \\ -b\,\dot{\theta} \end{bmatrix} \tag{39}$$

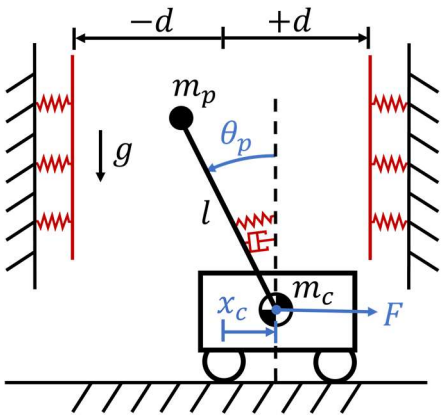

Fig. 3 States (blue) and parameters (black) of the cartpole system. The goal is to drive the cartpole to the origin in the presence of compliant walls and a torsional spring-damper.

A. *Cart-pole with Actuator Pre-Filter*

First, we examine the effect of the actuator pre-filter to control a cart-pole without walls or a torsional spring-damper. Data were sampled uniformly from a region of interest and lifted using radial basis functions placed via K-means++. Specifically, the dynamic ranges were bounded by

$$|x_c| \leq d, |\dot{x_c}| \leq 1 \tag{40}$$

$$|\theta_p| \leq \frac{\pi}{3}, |\dot{\theta_p}| \leq 1 \tag{41}$$

$$|F| \leq 10 \tag{42}$$

Multiple datasets were collected with varying actuator pre-filter time constants T and a parameter sweep to optimize controller performance determined the dilation factor and number of observables. A separate Koopman model was constructed for each value of T.

If the A matrix is exact, then the choice of T parameter should only impact A_w, the only nonzero element in the actuator state row. However, in this study, through the generation of data and the choice of observables, parameter T impacts the A matrices.

The x-position does not appear in the equations of motion, so it was excluded from the lifting and least-squares estimation (as described in Section 3B). The x-position dynamics were added back into the A matrix after model generation. The B matrix was obtained analytically from the actuator dynamics, and all hyperparameters were kept constant across models.

For the discrete-time linear system, the dynamics of the lifted state are given by

$$\boldsymbol{z}_{t+1} = \mathrm{A}\boldsymbol{z}_t + \mathrm{B}u_t \tag{43}$$

And the LQR performance index is defined as

$$J = \sum_{t=0}^{\infty} \boldsymbol{z}_t^T \mathrm{Q} \boldsymbol{z}_t + u_t^T R u_t \tag{44}$$

The state cost matrix Q is diagonal, with nonzero elements $Q_{ii} = 100$ corresponding exclusively to cartpole states (excluding F), and $R = 1$. No cost was assigned to errors in the observables. The optimal gain was obtained using MATLAB's dlqr function. Depending on the hyperparameters, the gains could not be obtained due to a lack of system controllability. This issue became more common with increasing numbers of observables. The Koopman models associated with $T = 1$ and $T = 10$ were eliminated from the analysis at this stage.

Finally, these Koopman LQR controllers were evaluated on 100 initial conditions sampled in a range similar to that of the training data. Each individual simulation was 12 seconds long. Figure 4 shows the average mean squared error and control input as a function of simulation time. Larger T values resulted in larger control efforts due to the slower actuator dynamics. Furthermore, on average the smaller T values settled faster to the desired state. Note, however, that there is the lower bound of the pre-filter time constant; the LQR gains could not be obtained for $T = 1$.

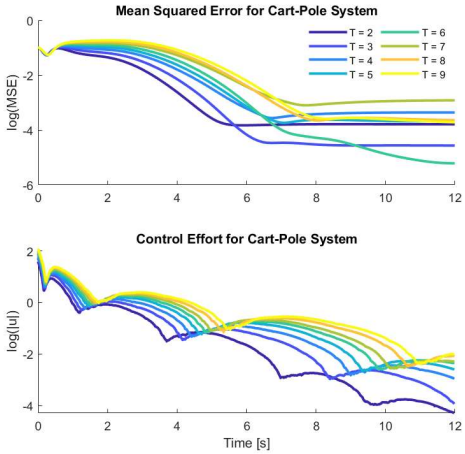

Fig. 4 Comparison plot of the mean squared error and control effort of Koopman-LQR controllers for a range of actuator pre-filter parameters T. Data is averaged over 100 trajectories and are shown varying throughout the duration of each simulation. (top) The desired position is the upright pendulum position at the origin, so MSE is simply the squared norm of the cartpole states. (bottom) Magnitude of the control input u, which linearly affects actuator state F. Results shown for the canonical cart-pole system.

The Koopman LQR controllers were reliable in stabilizing the cart-pole to the origin despite the varied T values, but not all were equally successful. The effects of T on the total LQR cost is shown in Figure 5 . Generally, we see higher LQR costs with increasing T due to larger control effort and increases in state error.

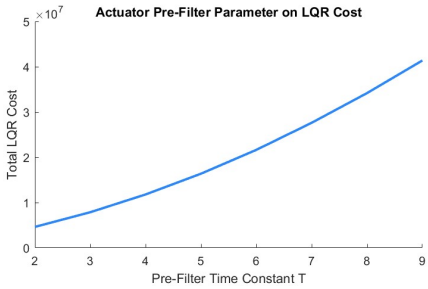

Fig. 5 Effects of the pre-filter time constant T on the total LQR cost, summed over 100 trajectories. Results shown for the canonical cart-pole system.

B. *Cart-pole with Compliant Walls and Actuator Pre-Filter*

We compare the performance of CCK controllers trained with and without knowledge of the walls over 1000 trajectories, sampled within the ranges given in equations (40-42), and using the same state and control weights. The MSE was computed as an average over the final second of each simulation. For 1000 six-second simulations, the wall-aware controller achieved a full-state MSE below 1 in 27.4% of trials, and below 10 in 69.5% of trials, yet 100% of trails had a position-only MSE below 0.1. This discrepancy indicates that the bulk of the full-state error is due to the velocity terms. Contrast this with the wall-unaware controller, who met all three thresholds in 16.5% of trials.

While the wall-aware controller was erratic and used rapid corrective actions, it was consistently able to bring the cart-pole close to the desired position. However, it was unable to arrive at the unstable equilibrium due to modeling errors

introduced by the wall dynamics. The wall-unaware could bring the cart-pole to the unstable equilibrium, but only if the trajectory was not disrupted by wall collisions.

C. Cart-pole with Compliant Walls, Torsional Spring-Damper, and Actuator Pre-Filter

Following the analysis with the canonical cart-pole, and the cart-pole with compliant walls, the system was extended to include a torsional spring-damper. The torsional spring-damper simplifies the control problem, facilitating the generation of Koopman models with identical hyperparameters that yield successful controllers. This isolates the effect of time constant T on controller performance.

Data were collected using the same method as before, and Koopman models were generated again with K-means++ placed radial basis functions. Fig. 6 compares the performance of four Koopman LQR controllers: Model A was trained on the canonical cart-pole, Model B was trained with the torsional spring and damper, and Models C and D were trained with knowledge of both the torsional spring-damper and the walls. All three used the same pre-filter time constant value ($T = 2$).

Model A, shown as the first column of Fig. 6, performed the worst. Without knowledge of the walls or torsional spring, it applied control inputs that caused it to bounce repeatedly between the walls. Both LQR controllers using Models B and C stabilized the system. However, Model B, lacking knowledge of the walls, initially moves further into the wall, and the unexpected wall contact force induces large-amplitude oscillations in θ. Model C, trained on data that includes wall dynamics, immediately moves away from the wall, demonstrating that the model has successfully captured and accounts for the wall interaction. The pole oscillated less due to the avoidance of the walls.

Finally, as a point of comparison, the rightmost column demonstrates an alternative method for obtaining the B matrix. Model D shares the same hyperparameters as Model C, but its B matrix is estimated from data, as is conventionally done with DMDc. The training data for Model D was generated identically to that of Model C. The dataset includes the actuator prefilter state, which alleviates the nonlinear control input problem that is the primary benefit of our proposed method, but also has randomized control inputs $u \leq |50|$. The inclusion of actuated dynamics introduces more variability into the training data, which can destabilize the learned Koopman model and degrade controller performance. The analytical approach is the more straightforward path to obtaining the B matrix.

Unlike in Section 4A., the inclusion of the compliant walls made it difficult to generate many Koopman models with the same hyperparameters whose control performance was satisfactory. Nevertheless, three controllers were found with the same hyperparameters who were consistently capable of bringing the cart-pole to the desired equilibrium. The eigenvalues of these Koopman models are shown in Fig. 7. Shown in blue are the eigenvalues associated with the dynamics of prefilter states w. From the pre-filter dynamics (32), we see A_w, the section of the A matrix associated with w, is given by

$$w_{t+1} = A_w w_t = \left(w_t - \frac{\Delta_t w_t}{T}\right) = \left(1 - \frac{\Delta_t}{T}\right) w_t. \quad (45)$$

Thus, as T increases in value, this pole gets pushed closer to the unit circle. As T approaches the simulation time Δ_t, the poles get pushed increasingly towards the origin along the real line.

The relative performance of these three Koopman LQR controllers is shown in Figures 8 and 9 for a set of 100 trajectories. For this system, the larger time constant controller was able to settle faster than the smaller time constant controllers. The aggregate LQR cost still follows the trend that smaller prefilters parameters yield controllers that incur less cost. The LQR cost metric is heavily weighted against squared errors in state, but due to generally small state errors overall, the large initial state error and control inputs for the larger T case at the start of the simulations lead to an overall higher aggregate cost.

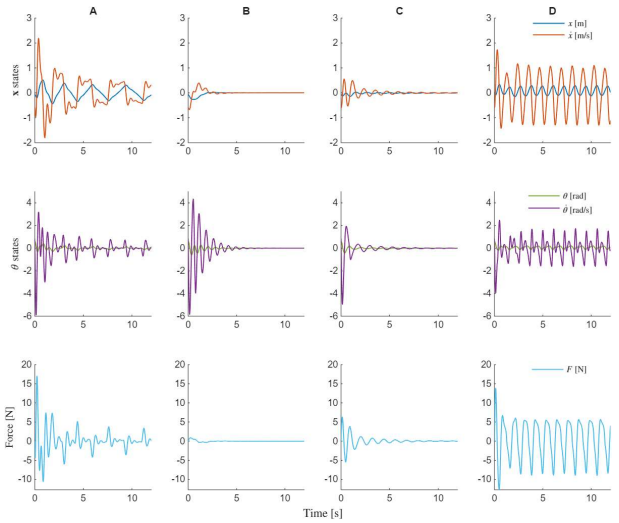

Fig. 6 Plots of states for four Koopman LQR controllers, evaluated in a simulation with both torsional spring-damper and compliant walls. Models A, B, and C are CCK models in which the B matrix is obtained analytically, while Model D follows the conventional approach of obtaining the B matrix from data. Model A is trained on data from the canonical cart-pole system, Model B on data incorporating the torsional spring-damper, and Models C and D on data including both the torsional spring-damper and wall dynamics.

Conclusion

In conclusion, we present the method of actuator pre-filtering and Koopman lifting linearization to enable the use of optimal linear control techniques to systems where typically such linear techniques are not applicable (e.g. systems undergoing contact). The inclusion of actuator dynamics alleviates the state dependent nature of the control input in the traditional system. However, the parameters used to delay the control input have a noticeable effect in control performance. LQR costs are shown to decrease with smaller time constants, but volatility in the system may make Koopman models more difficult to construct with such fast-changing dynamics, depending on the sampling rate and simulation fidelity. Nevertheless, the use of actuator prefilters enables the construction of Control Coherent Koopman models without needing additional compliance within the actuator subsystem, making the method relevant to a broader range of applications.

The CCK modelling and Koopman MPC have been used to control a planar pushing in simulation and hardware, and a rimless wheel system [19]. While these systems are

relatively simple, and there exists a curse of dimensionality issue with increasing number of actuators, Koopman model dimension does not scale with the number of contact modes. Moreover, Koopman models have been generated for complicated legged systems with high degrees of freedom [20]. CCK and actuator pre-filtering approach complements ongoing work in extending Koopman control techniques to complex systems undergoing contact.

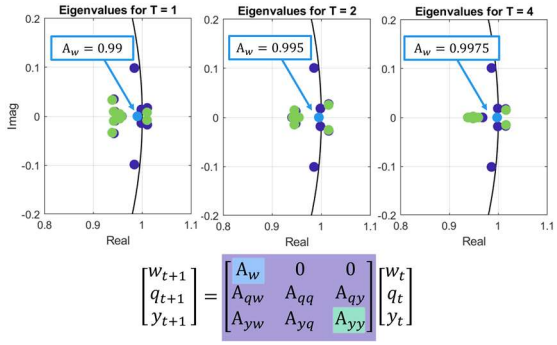

Fig. 7 Poles of Koopman models for the cart-pole system with walls and for varying T values. In blue are the poles associated with the actuator pre-filter, in green are the poles associated with the observables, and in purple are the remaining eigenvalues.

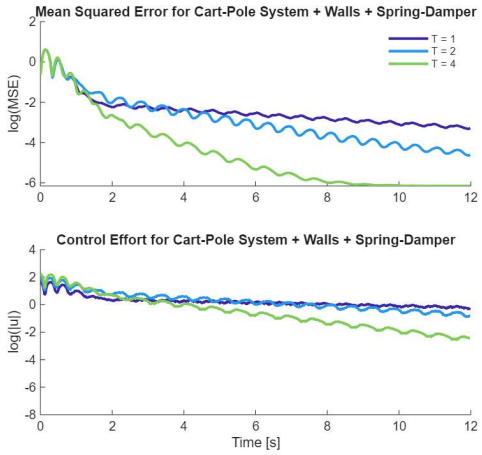

Fig. 8 Comparison plot of the mean squared error and control effort of Koopman LQR controllers for a range of actuator pre-filter parameters T. Data is averaged over 100 trajectories and are shown varying throughout the duration of each simulation. Results shown for the cart-pole system with compliant walls and a torsional spring-damper.

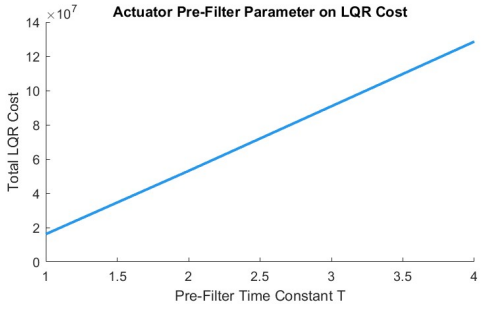

Fig. 9 Effects of the pre-filter time constant T on the total LQR cost, summed over 100 trajectories. Results shown for the cart-pole system with compliant walls and a torsional spring-damper.

REFERENCES

[1] Wensing, P. M. et al. Optimization-Based Control for Dynamic Legged Robots. Preprint at https://doi.org/10.48550/arXiv.2211.11644 (2022).

[2] Koolen, T., De Boer, T., Rebula, J., Goswami, A. & Pratt, J. Capturability-based analysis and control of legged locomotion, Part 1: Theory and application to three simple gait models. The International Journal of Robotics Research 31, 1094–1113 (2012).

[3] Mason, M. T. Mechanics and Planning of Manipulator Pushing Operations. The International Journal of Robotics Research 5, 53–71 (1986).

[4] Hogan, F. R., Grau, E. R. & Rodriguez, A. Reactive Planar Manipulation with Convex Hybrid MPC. in 2018 IEEE International Conference on Robotics and Automation (ICRA) 247–253 (2018). doi:10.1109/ICRA.2018.8461175.

[5] H. Asada, "Global, Unified Representation of Heterogenous Robot Dynamics Using Composition Operators: A Koopman Direct Encoding Method", IEEE/ASME Transactions on Mechatronics, Vol.28, Issue 5, pp. 2633-2644, DOI: 10.1109/TMECH.2023.3253599, February (2023).

[6] B. O. Koopman, "Hamiltonian Systems and Transformations in Hilbert Space," Proceedings of the National Academy of Sciences of the United States of America, vol. 17, no. 5, pp. 315–318, 1931.

[7] A. Mauroy, I. Mezic, and Y. Susuki, "The Koopman Operator in Systems and Control", Springer, 2020.

[8] I. Abraham and T. D. Murphey, "Active Learning of Dynamics for Data-Driven Control Using Koopman Operators," IEEE Transactions on Robotics, vol. 35, no. 5, pp. 1071–1083, 2019.

[9] D. A. Haggerty, M. J. Banks, E. Kamenar, A. B. Cao, P. C. Curtis, I. Mezić, and E.W. Hawkes, "Control of Soft robots with Inertial Dynamics", Science Robotics, Vol 8, Issue 81, DOI: 10.1126/scirobotics.add6864, 2023

[10] J. L. Proctor, S. L. Brunton, and J. N. Kutz, "Dynamic Mode Decomposition with Control," SIAM Journal on Applied Dynamical Systems, vol. 15, no. 1, pp. 142–161, 2016.

[11] J. L. Proctor, S. L. Brunton, and J. N. Kutz, "Generalizing Koopman Theory to Allow for Inputs and Control," SIAM Journal on Applied Dynamical Systems, vol. 17, no. 1, pp. 909–930, 2018.

[12] D. Bruder, X. Fu, and R. Vasudevan, "Advantages of Bilinear Koopman Realizations for the Modeling and Control of Systems With Unknown Dynamics," IEEE Robotics and Automation Letters, vol. 6, no. 3, pp. 4369–4376, 2021.

[13] S. Otto, S. Peitz, and C. Rowley, 'Learning Bilinear Models of Actuated Koopman Generators from Partially Observed Trajectories', SIAM Journal on Applied Dynamical Systems, vol. 23, no. 1, pp. 885–923, 2024

[14] H. Asada and J. Solano-Castellanos, "Control-Coherent Koopman Modeling: A Physical Modeling Approach", Proc. of the 63rd IEEE Conference on Decision and Control (CDC), Milan, December 2024.

[15] H. Asada, "An Actuator Pre-Filtering Approach to Control-Coherent Koopman Modeling: Extending Koopman Operators to Systems with Control", IEEE Control Systems Letters, Vol. 9, pp 2067 – 2072, DOI: 10.1109/LCSYS.2025.3582608, June 2025.

[16] E. Yeung, S. Kundu, and N. Hodas, "Learning Deep Neural Network Representations for Koopman Operators of Nonlinear Dynamical Systems". in 2019 American Control Conference (ACC) 4832–4839 (2019). doi:10.23919/ACC.2019.8815339.

[17] H. Asada and J.-J. Slotine, "Robot Analysis and Control", Wiley, 1985.

[18] C. O'Neill and H. H. Asada, "Koopman Dynamic Modeling for Global and Unified Representations of Rigid Body Systems Making and Breaking Contac https://www.linkedin.com/in/jasmine-terrones/ t," 2024 IEEE/RSJ International Conference on Intelligent Robots and Systems (IROS), Abu Dhabi, United Arab Emirates,2024, pp. 709-716, doi: 10.1109/IROS58592.2024.10801737.

[19] C. O'Neill, J. Terrones, and H. H. Asada, "Koopman global linearization of contact dynamics for robot locomotion and manipulation enables elaborate control," Nov. 09, 2025, *arXiv*: arXiv:2511.06515. doi: 10.48550/arXiv.2511.06515.

[20] F. Li, A. Abuduweili, Y. Sun, R. Chen, W. Zhao, and C. Liu, "Continual Learning and Lifting of Koopman Dynamics for Linear Control of Legged Robots," Jun. 03, 2025, *arXiv*: arXiv:2411.14321. doi: 10.48550/arXiv.2411.14321.